TRANSONIC LIMIT CYCLE OSCILLATION ANALYSIS OF AEROSTABIL WIND TUNNEL MODEL

Hitoshi Arizono[1], **Kenichi Saitoh**[1], **Masato Tamayama**[1]

[1]Japan Aerospace Exploration Agency
6-13-1 Osawa Mitaka Tokyo 1810015 Japan
arizono.hitoshi@jaxa.jp, saitoh.kenichi@jaxa.jp, tamayama.masato@jaxa.jp

Keywords: transonic aerodynamics, limit cycle oscillation, computational fluid dynamics

Abstract: The aerodynamic nonlinearities such as large shock motions and flow separation are one of the cause of the limit cycle oscillations. It is difficult to predict the amplitude of the limit cycle oscillations. This paper presents the prediction of the amplitude of the limit cycle oscillations using the state-of-the-art CFD solver.

1 INTRODUCTION

Limit cycle oscillations (LCO) are usually defined as self-sustained oscillations with limited amplitudes. In reference [1], the type of LCO are categorized: (1) airfoils with stiffness nonlinearities, (2) delta wings with geometrical plate nonlinearities, (3) very high aspect ratio wings with both structural and aerodynamic nonlinearities, (4) nonlinear structural damping and (5) aerodynamic flows with large shock motions and flow separation.

In the transonic region, the presence of shocks on the wing surface introduces strong aerodynamic nonlinearities. The prediction of LCO amplitudes is much more difficult than the related problem of predicting the linear flutter boundary [2]. Stickan et al. [3] presented the LCO simulations of Aerostabil wing. The amplitudes of LCO by the simulation could not meet with the results of experiments.

Recent Computational Fluid Dynamics (CFD) solver can estimate the drag and the complicated flow such as the high lift configuration. This paper presents the prediction of LCO amplitude of Aerostabil wind tunnel model using the state-of-the-art CFD solver which is developed at JAXA.

2 AEROSTABIL WIND TUNNEL MODEL

Figure 1 shows the geometry of Aerostabil wind tunnel model. The root chord length is 0.242 m and the tip chord length is 0.099 m. The span length without wing tip is 0.601 m. The leading edge sweepback angle is 32 deg. The reference chord length is c_{ref} is 0.183 m. The differential pressure transducers are installed in three span stations. The accelerometers are also installed in the model. The detail geometry of Aerostabil wind tunnel model is in reference [4].

Aerostabil wind tunnel model was tested in the Transonic Windtunnel in Goettingen (DNW-TWG). The results of the wind tunnel tests are presented in reference [4].

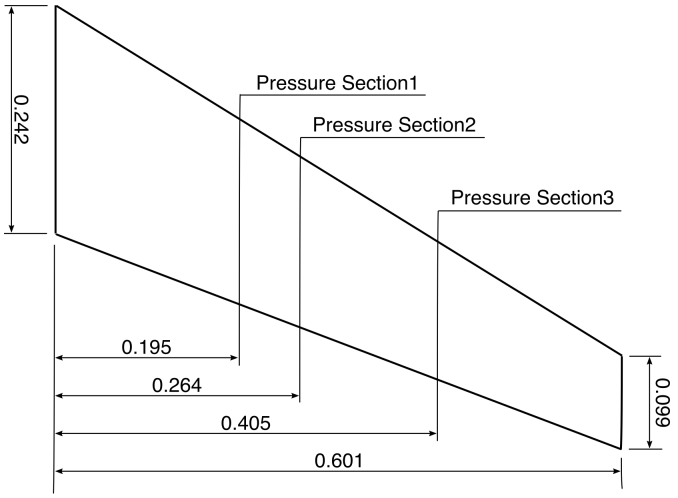

Figure 1: Geometry of Aerostabil wind tunnel model

3 NUMERICAL METHODS

FaSTAR [5] is used for the aerodynamic solver. FaSTAR solves the Reynolds-Averaged Navier-Stokes (RANS) equations on the unstructured grid using a cell-centered finite volume method. The Harten-Lax-van Lee-Wada (HLLEW) method [6] is used for the numerical flux computations. Lower/Upper Symmetric Gauss-Seidel (LU-SGS) implicit method is used for time integration. The second order spatial accuracy is realized by a linear reconstruction of the primitive variables with Venkatakrishnan's limiter [7] and Unstructured MUSCL scheme (U-MUSCL). As for trubulence model, Spalart-Allmaras model [8] and Menter's shear stress transport k-ω model (SST) [9] can be used. The equations for the turbulence models are also solved using the 2nd order scheme. In the present study, Spalart-Allmaras model is used and trubulent transition is not taken into account.

The aeroelastic equations are needed to solve the dynamic aeroelastic problems. The following subroutines are added to FaSTAR; (1) read the vibration characteristics, (2) calculate pressures on the surfaces, (3) solve the aeroelastic equations, (4) move surface grids, (5) move spatial grid. The subroutines from (2) to (5) are used in each time step. The governing aeroelastic equations of motion are solved using the modal approach. These equations of motion are derived by assuming that the deformation of the body under consideration can be described by a separation of variables involving the summation of free vibration modes weighted by generalized displacements. The integration of the governing equations are employed the Wilson's θ method.

Figure 2 shows the CFD grid around model which is generated using MEGG3D [10]. The number of grid points are about 2.4 million and the number of cells are 7.1 million. The farfield extends approximately 130 reference chord length from the wing surface.

Table 1 and Figure 3 show the modal characteristics of Aerstabil wing model. These data are based on the vibration tests in reference [4]. The mode shapes are interpolated to the CFD surface grid using Thin Plate Spline [11].

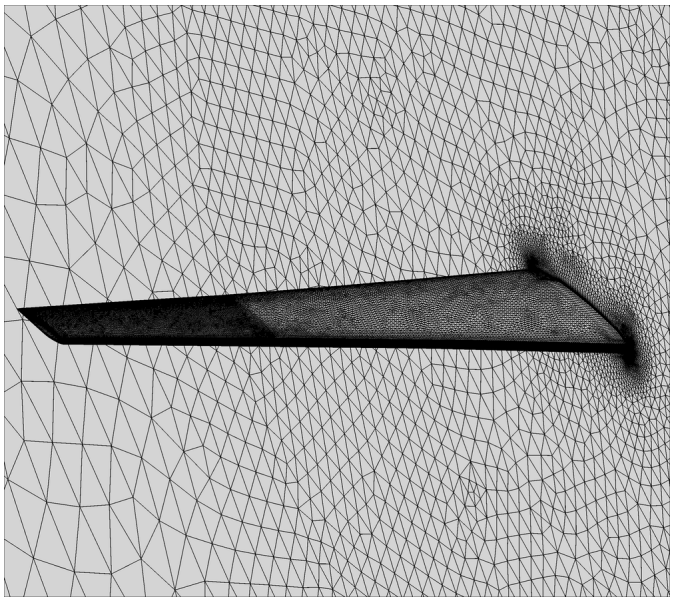

Figure 2: CFD grid around model

Mode No.	Mode Description	Frequency (Hz)
1	1st bending	37.81
2	2nd bending	112.85
3	3rd bending	241.85
4	1st torsion	272.60
5	4th bending	374.50
6	2nd torsion	420.00

Table 1: Modal characteristics of Aerstabil wind tunnel model

4 NUMERICAL RESULTS

4.1 Static aeroelastic simulations

The static simulation results are shown in this section. The flow condition is Mach number $Ma = 0.819$, angle of attack $\alpha = 0.0$ deg, Reynolds number $Re = 1.33 \times 10^6$ and Sutherland number $Su_0 = 0.36$.

The pressure coefficients at each pressure tap section are shown in Figure 4. The spatial contour of the pressure coefficients and the Mach number at each pressure tap section are shown in Figure 5 and 6. The predicted strength of shock at the outboard wing is weak as compared with the experiment.

4.2 LCO simulations

The LCO simulation results are shown in this section. The flow condition is Mach number $Ma = 0.865$, angle of attack $\alpha = 2.69$ deg, Reynolds number $Re = 1.69 \times 10^6$ and Sutherland

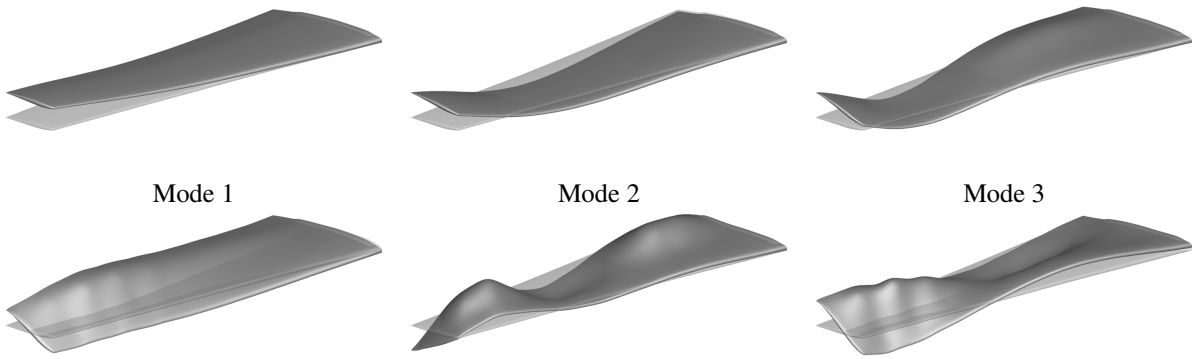

Mode 1 Mode 2 Mode 3

Mode 4 Mode 5 Mode 6

Figure 3: Mode shapes of Aerostabil wind tunnel model

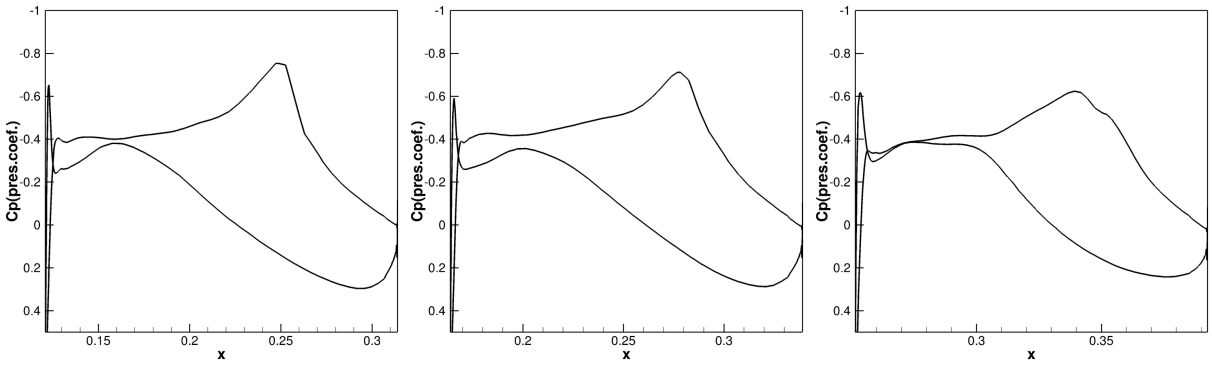

y=0.195 m y=0.264 m y=0.405 m

Figure 4: Pressure coefficients on the surface of model

number $Su_0 = 0.36$.

Figure 7 and 8 show the time history of the generalized modal displacements and the displacement of the position at the accelerometer 6. The amplitude is almost constant (22 mm), but it is larger than the results of the experiments (10 mm). The spatial contour of the Mach number at the top and bottom of the amplitude are shown in Figure 9. The shock moves back and forth during oscillation and the separation region after the shock expand as the strength of the shock.

5 CONCLUSIONS

The static and dynamic aeroelastic simulations of Aerostabil wind tunnel model were performed with FaSTAR solver. The amplitudes of LCO using the current aeroelastic solver could not predict exactly. For the future, the effects of the grid resolution, the turbulence models and the initial conditions will be investigated.

REFERENCES

[1] Earl H. Dowell. *A Modern Course in Aeroelasticity*. Kluwer Academic Publishers, 2004.

[2] Oddvar O. Bendiksen. Transonic limit cycle flutter/lco. In *45th AIAA/ASME/ASCE/AHS/ASC Structures, Structural Dynamics and Materials Conference*, AIAA Paper 2004-1694, April 2004.

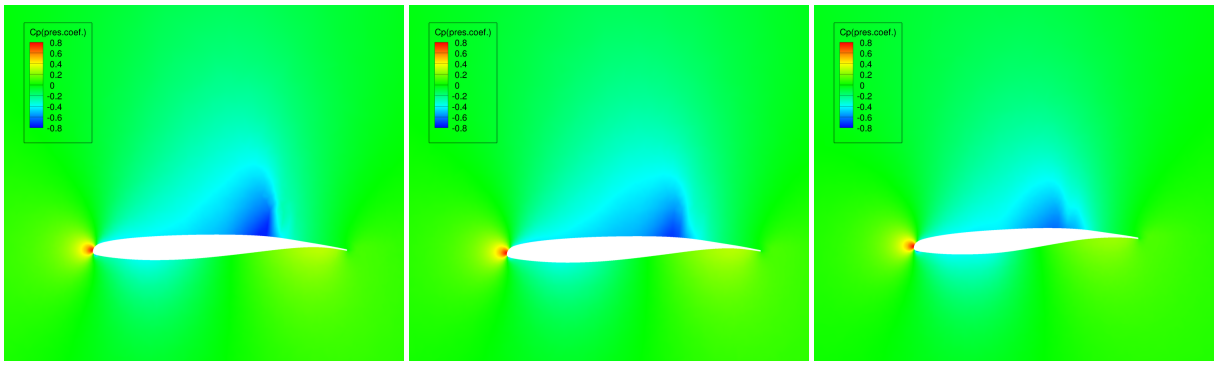

y=0.195 m y=0.264 m y=0.405 m

Figure 5: Spatial pressure coefficient contour

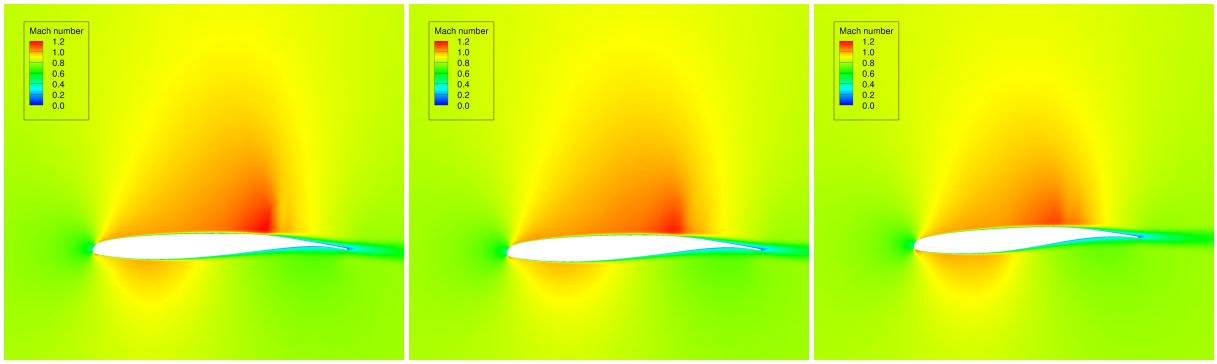

y=0.195 m y=0.264 m y=0.405 m

Figure 6: Spatial Mach number contour

[3] Bernd Stickan, Johannes Dillinger, and Günter Schewe. Computational aeroelastic investigation of a transonic limit-cycle-oscillation experiment at a transport aircraft wing model. *Journal of Fluids and Structures*, 49:223–241, August 2014.

[4] G. Dietz, Günter Schewe, F. Kießling, and M. Sinapius. Limit-cycle-oscillation experiments at a transport aircraft wing model. In *International Forum on Aeroelasticity and Structural Dynamics 2003*, June 2003.

[5] Atsushi Hashimoto, Keiichi Murakami, Takashi Aoyama, and Keiichi Ishiko. Toward the fastest unstructured cfd code "fastar". In *50th AIAA Aerospace Sciences Meeting*, AIAA Paper 2012-1075, January 2012.

[6] Shigeru Obayashi and Guru P. Guruswamy. Convergence acceleration of a navier-stokes solver for efficient static aeroelastic computations. *AIAA Journal*, 35(6):1134–1141, June 1995.

[7] V. Venkatakrishnan. Convergence to steady state solutions of the euler equations on unstructured grids with limiters. *Journal of Computational Physics*, 118(1):120–130, April 1995.

[8] P. R. Spalart and S. R. Allmaras. A one-equation turbulence model for aerodynamic flows. In *30th Aerospace Sciences Meeting and Exhibit*, AIAA Paper 92-0439, January 1992.

[9] F. R. Menter, M. Kuntz, and R. Langtry. Ten years of industrial experience with the sst turbulence model. In *Turbulence, Heat and Mass Transfer IV*, October 2003.

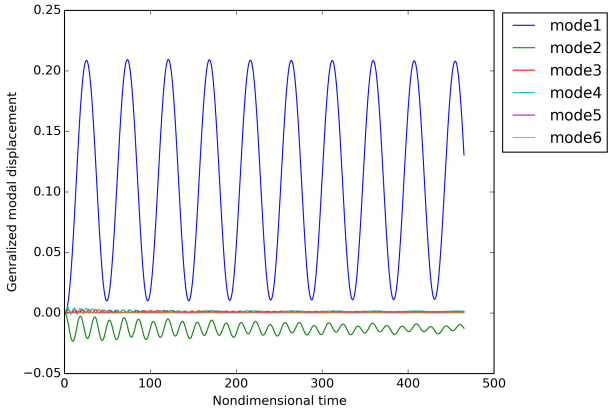

Figure 7: Generalized modal diplacement

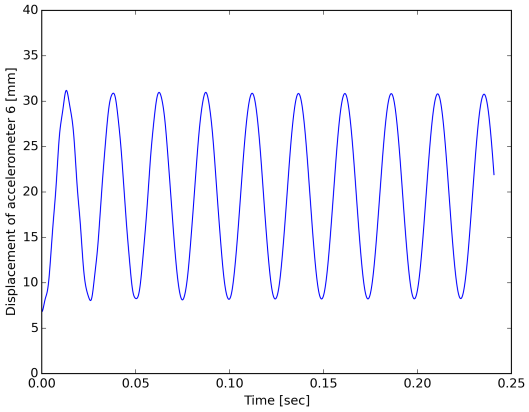

Figure 8: Displacement of position of accelerometer 6

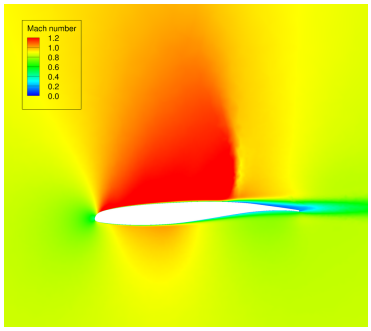

top of amplitude

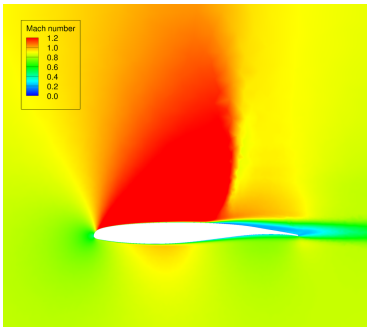

bottom of amplitude

Figure 9: Mach number contour during oscillation

[10] Yasushi Ito and Kazuhiro Nakahashi. Improvements in the reliability and quality of unstructured hybrid mesh generation. *Numerical Methods in Fluids*, 45(1):79–108, May 2004.

[11] Marilyn J. Smith, Dewey H. Hodges, and Carlos E. S. Cesnik. Evaluation of computational algorithms suitable for fluid-structure interactions. *Journal of Aircraft*, 37(2):282–294, March–April 2000.